THE JOURNAL OF PHYSICAL CHEMISTRY LETTERS
A JOURNAL OF THE AMERICAN CHEMICAL SOCIETY

pubs.acs.org/JPCL Letter

Synthesis of Two-Dimensional $CsPb_2X_5$ (X = Br and I) with a Stable Structure and Tunable Bandgap by $CsPbX_3$ Phase Separation

Mei Li, Shang Peng, Shiyu Fang, Yu Gong, Dongliang Yang, Kejun Bu, Bingyan Liu, Hui Luo, Songhao Guo, Junlong Li, Hao Wang, Yufeng Liu, Sheng Jiang, Chuanlong Lin,* and Xujie Lü*

Cite This: *J. Phys. Chem. Lett.* 2022, 13, 2555−2562 Read Online

ABSTRACT: Perovskite-related materials with various dimensionalities have attracted sustained attention owing to their extraordinary electronic and optoelectronic properties, but it is still challenging in the synthesis of compounds with desired compositions and structures. Herein, a two-dimensional (2D) $CsPb_2I_5$ perovskite has been synthesized by the conversion of $CsPbI_3$ at high-pressure and high-temperature (high $P-T$) conditions, which is quenchable at ambient conditions. *In situ* synchrotron X-ray diffraction shows that high-pressure monoclinic $CsPbI_3$ converts into tetragonal $CsPb_2I_5$ and cubic CsI at 8.7 GPa upon heating from 644 to 666 K. Keeping the tetragonal structure stable, $CsPb_2I_5$ exhibits tunable optical properties with the bandgap changing from ∼2.4 eV at ambient pressure to ∼1.4 eV at 36.9 GPa. Further experiments demonstrate similar structural evolution in the typical three-dimensional $CsPbBr_3$ perovskite into 2D $CsPb_2Br_5$ at high $P-T$ conditions, indicating that the conversion of $CsPbX_3$ (X = Br and I) into $CsPb_2X_5$ is ubiquitous.

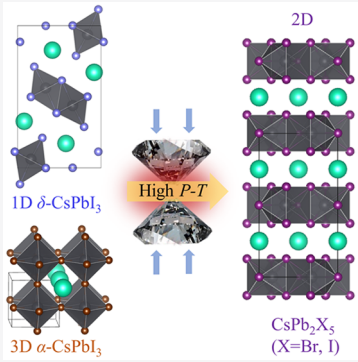

Halide perovskites, possessing flexible lattices and exceptional optoelectronic properties, have achieved remarkable performance in the applications of solar cells,[1] photodetectors,[2] and light-emitting diodes (LEDs)[3] but still suffer from problems, like the instability of ionic lattices.[4−6] Two-dimensional (2D) inorganic $CsPb_2X_5$, as a derivative of $CsPbX_3$ perovskite, has attracted increasing attention owing to its unique optical properties and quantum confinement effects.[7−10] They exhibit higher stability against moisture in an air environment, which benefits from the intrinsic structure with a layered arrangement of Pb−X polyhedron and Cs^+.[11] Research of the fundamental structure−property correlation of $CsPb_2X_5$ could bring out the design inspiration of novel materials. Although $CsPb_2X_5$ has been shown to exhibit enhanced optical properties,[8,9,11] problems regarding underlying mechanisms of the structural evolution and properties remain unclear.[12−16] For example, 2D $CsPb_2Br_5$ has been previously synthesized, while 2D $CsPb_2I_5$ was only theoretically predicted, waiting to be validated experimentally. This provokes the exploration of more universal methods for the synthesis of 2D $CsPb_2X_5$.

For the synthesis of 2D perovskite-like analogue $CsPb_2X_5$, a wide variety of methods have been employed. The direct synthesis starts from the raw precursors, and the structures and properties of the resulting products are highly dependent upon the CsX/PbX_2 stoichiometric ratio and the thermodynamic conditions but still lacking general principles to follow. The post-synthesis, breaking up the three-dimensional (3D) metal halide perovskite network into low-dimensional perovskite-related networks, is an effective strategy, which has been proven by a variety of experimental results.[17] For instance, the ligand-assisted excess $PbBr_2$ insertion or adding extra bromide source (such as NaBr) could transform $CsPbBr_3$ to Br-rich $CsPb_2Br_5$[18−22] with the chemical reaction of $CsPbX_3 + PbX_2 \rightarrow CsPb_2X_5$; CsX stripping is also a promising approach by means of the ultrahigh solubility of CsX in polar solvents, following the pathway: $CsPbX_3 \rightarrow CsPb_2X_5 + CsX$.[18−24] However, the traditional synthesis methods usually require several raw precursors, follow complex chemical reaction steps, and produce $CsPb_2X_5$ accompanied by impurities and defects in the products. In particular, these methods require capping ligand mediations (such as oleic acid and oleyl amine) or multiple solvents (such as dimethylformamide and tetrahydrofuran) for different purposes, i.e., decreasing the surface energy and stabilizing the crystal structure.[25−27] Here, we present a new synthesis process of $CsPb_2X_5$ under high pressure and thermal treatments via the direct-phase separation of $CsPbX_3$, which is distinguished from conventional methods.

Pressure, as a thermodynamic variable, provides an effective knob to synthesize novel materials, which cannot be achieved using traditional techniques.[28−33] In combination with *in situ* characterization methods, high-pressure research could provide a better fundamental understanding of the chemical reaction

Received: January 13, 2022
Accepted: March 11, 2022

https://doi.org/10.1021/acs.jpclett.2c00116
J. Phys. Chem. Lett. 2022, 13, 2555−2562

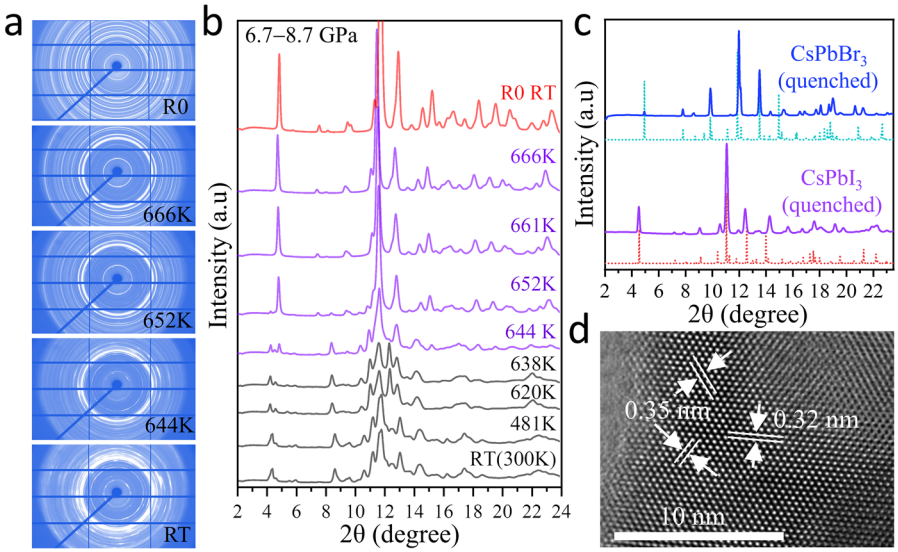

Figure 1. Structural evolution of $CsPbI_3$ upon heating at high pressure. (a) 2D diffraction images and (b) one-dimensional (1D) integrated XRD profiles at different temperatures. (c) XRD patterns of high $P-T$ phases obtained by heating $CsPbBr_3$ and $CsPbI_3$ at high pressure in comparison to calculated XRD patterns (dot lines) using the tetragonal structure predicated theoretically (material project, mp-1238789). (d) Typical HRTEM image of the high $P-T$ phase of $CsPb_2I_5$.

and crystal growth mechanisms.[34−37] Previous research has reported that the perovskite $MgSiO_3$[38] and its traditional low-pressure analogues (such as $NaMgF_3$[39] and $MgGeO_3$[40]) could be dissociated into AB_2X_5 ($P2_1/c$ type) and BX (CsCl type) under high pressures, which have been reported in ABX_3 systems by following the transition sequence of perovskite → post-perovskite → U_2S_3-type post-post-perovskite → $P2_1/c$-type AB_2X_5. This provides an alternative method to synthesize 2D perovskite-like analogue $CsPb_2X_5$ formed from 3D perovskite $CsPbX_3$ at high-pressure and high-temperature ($P-T$) conditions. In this work, we report the synthesis of 2D $CsPb_2X_5$ (X = Br and I) by the direct conversion of $CsPbI_3$ at high $P-T$ conditions with the reaction of $2CsPbX_3 \rightarrow CsPb_2X_5 + CsX$. $CsPb_2I_5$ is focused, because the synthesis using the traditional methods is rarely reported. Variations of structural and optical properties were systematically investigated using *in situ* synchrotron X-ray diffraction (XRD) and ultraviolet−visible (UV−vis) absorption spectroscopy. Newly obtained $CsPb_2I_5$ exhibits flexible optical properties while keeping the tetragonal structure stable up to 33.3 GPa. Note that both $CsPbI_3$ and $CsPbBr_3$ display a similar transformation into 2D $CsPb_2Br_5$, indicating that the phase separation of $CsPbX_3$ (X = Br and I) is a common phenomenon at high $P-T$ conditions. This work not only presents a general method for the synthesis of 2D perovskite derivatives at high $P-T$ conditions, which is unachievable using traditional methods, but also provides deep insight into the formation mechanism.

At ambient conditions, δ-$CsPbI_3$ is the stable phase and adopts an orthorhombic structure with space group *Pnma* and lattice constants of a = 10.4342(7) Å, b = 4.7905(3) Å, and c = 17.7761(1) Å.[41] The crystal structure of δ-$CsPbI_3$ is built by double chains of edge-sharing $[PbI_6]^{4-}$ octahedra separated by Cs^+ cations and transforms to a typical 3D perovskite structure featured with the corner-sharing $[BX_6]^{4-}$ octahedra below 1 GPa and above 370 K.[42] In this work, the $CsPbI_3$ crystal was loaded into the chamber of a diamond anvil cell (DAC) and first compressed up to around 8.7 GPa. XRD patterns show a phase transformation occurring at ∼4 GPa from a δ-$CsPbI_3$ phase to a high-pressure monoclinic structure (Figure S1 of the Supporting Information), consistent with the previous reports.[43,44] Keeping the pressure at 8.7 GPa, the monoclinic $CsPbI_3$ sample was heated to investigate the structural evolution with the temperature using externally heated DACs. As shown in Figure 1, the high-pressure monoclinic phase is kept stable up to 638 K with the temperature increasing. Above 638 K, new diffraction peaks emerge with the disappearance of parent peaks, indicating a phase transition. The high $P-T$ phase co-exists with the room-temperature (RT) monoclinic phase at temperatures from 644 to 652 K, and the high $P-T$ phase was observed above 660 K with homogeneous diffraction rings (panels a and b of Figure 1). The sample was then cooled, and the high $P-T$ phase can be quenched to room temperature. The pressure changes slightly from 8.7 to 6.7 GPa during heating and cooling processes. The high $P-T$ phase is reserved during the pressure release (Figure S2 of the Supporting Information). The high $P-T$ phase formed from $CsPbI_3$ cannot be assigned to the post-perovskite or any previously reported phase in ABX_3, such as $CsGeI_3$[45] and $EuNbO_3$.[28] Using the program Dicvol, most of the diffraction peaks can be well-indexed into a tetragonal phase with the space group *I*4/*mcm*. The feature reflections fit well into calculated XRD patterns of $CsPb_2I_5$ (Figure 1c), indicating the formation of $CsPb_2I_5$ by conversion of $CsPbI_3$ with the following process of $2CsPbI_3 \rightarrow CsPb_2I_5 + CsI$. The peaks at 19.1° together with some weak peaks can be attributed to CsI with a = 4.57 Å, consistent with previous reports.[46]

The structural evolution at high $P-T$ conditions is repeatable in $CsPbI_3$, and a similar process was observed in $CsPbBr_3$ upon heating up to 623 K at 8.3 GPa (Figure 1c and Figures S3 and S4 of the Supporting Information). $CsPb_2Br_5$ acts as an extension of the new approach under high $P-T$ conditions, revealing that the formation of $CsPb_2X_5$ by phase separation of $CsPbX_3$ at high $P-T$ conditions is reliable. Figure 1d and Figure S5 of the Supporting Information show the high-resolution transmission electron microscopy (HRTEM) images of the recovered sample. The interfringe distances of 0.32 and 0.35 nm could be indexed to the (220) and (114)

https://doi.org/10.1021/acs.jpclett.2c00116
J. Phys. Chem. Lett. 2022, 13, 2555−2562

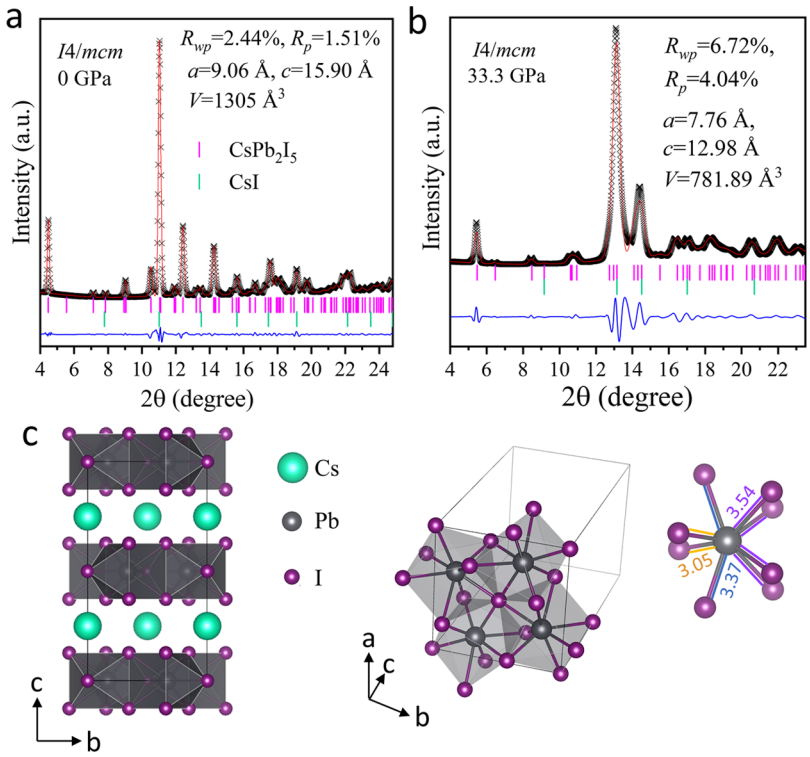

Figure 2. Crystal structure of $CsPb_2I_5$ at (a) 0 GPa and (b) 33.3 GPa. The ticks at the bottom indicate $CsPb_2X_5$ (red) and CsI (green) Bragg positions, respectively. (c) Crystal structural schematics of $CsPb_2X_5$.

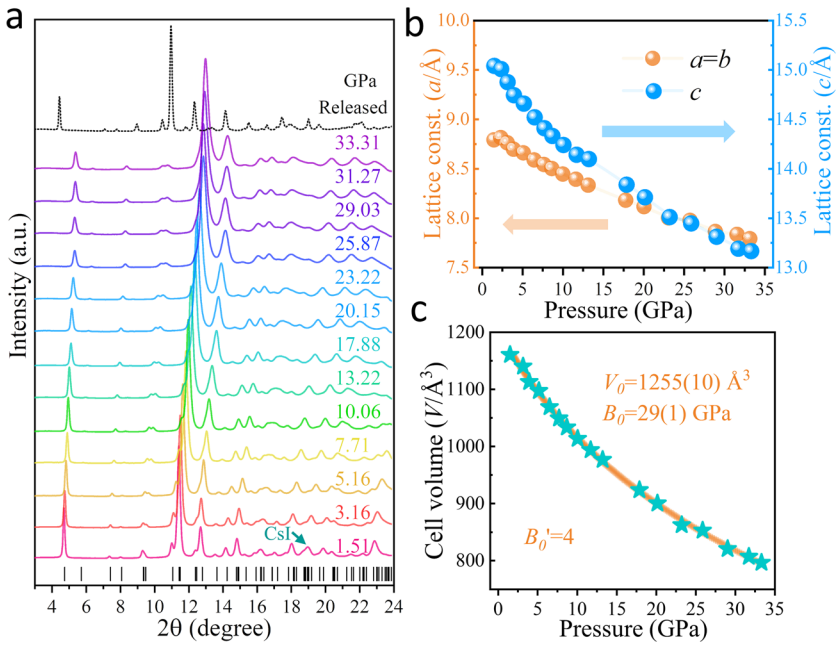

Figure 3. *In situ* structural characterizations of $CsPb_2I_5$ under high pressures. (a) XRD patterns at selected pressures. The green arrow represents the recognizable peak of CsI. The dashed line is the pattern for the recovered sample from high $P-T$ conditions. (b) Lattice parameters and (c) cell volume as a function of the pressure.

lattice planes of tetragonal $CsPb_2I_5$, respectively. The recovered sample with uniform surface morphology was demonstrated by scanning electron microscopy (SEM), and the homogeneous elemental distributions was quantified by energy-dispersive spectroscopy mapping (Figure S6 of the Supporting Information).

Figure 2a and Figure S7 of the Supporting Information show the refinement results of XRD patterns of $CsPb_2X_5$ (X = Br and I). $CsPb_2X_5$ adopts a tetragonal structure with space group *I*4/*mcm*, yielding the lattice constants of $a = b = 9.060(1)$ Å, $c = 15.901(2)$ Å, and $V = 1305.3(4)$ Å^3 for $CsPb_2I_5$ and $a = b = 8.4781(1)$ Å, $c = 15.1589(9)$ Å, and $V = 1089.60(5)$ Å^3 for $CsPb_2Br_5$. The lattice parameters are slightly smaller than those

https://doi.org/10.1021/acs.jpclett.2c00116
J. Phys. Chem. Lett. 2022, 13, 2555−2562

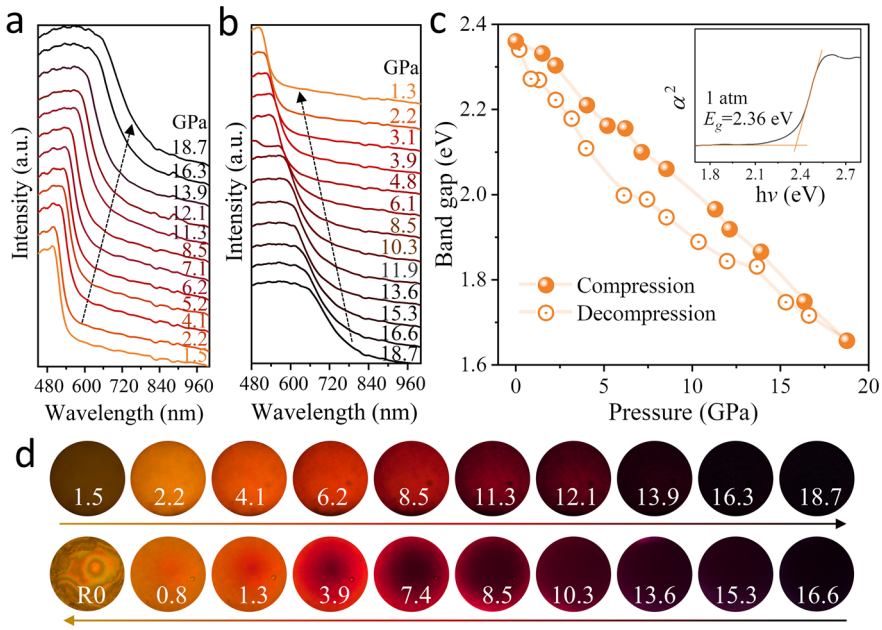

Figure 4. Optical properties of $CsPb_2I_5$ under pressure. Selected UV−vis absorption spectra during (a) compression and (b) decompression. (c) Bandgap evolution under the compression−decompression cycling. The inset shows the Tauc plot at ambient conditions. (d) Representative optical micrographs at selected pressures.

of the theoretical calculation. This may be due to the stress relaxation of $CsPb_2I_5$ quenched from high pressure. The tetragonal structure of $CsPb_2I_5$ is a quasi-2D structure, as shown in Figure 2c. One layer of Cs cations is sandwiched between two layers of the Pb_2I_5 coordination polyhedron, wherein the Pb_2I_5 layers consist of Pb atoms coordinated with eight I anions, different from the perovskite structure with edge- or corner-sharing octahedra. In the Pb_2I_5 polyhedral layer, each Pb−I polyhedron is connected by faces and has two short bonds of 3.05 Å, two bonds of 3.37 Å, and four long bonds of 3.54 Å, respectively.

The structural variations of $CsPb_2I_5$ under high pressures were further investigated. Upon compression, all diffraction peaks shift to higher 2θ angles as a result of the lattice contraction. No new Bragg peaks can be observed (Figure 3a), implying that $CsPb_2I_5$ keeps the tetrahedral structure stable up to 33.3 GPa. The *d*-spacing decreases continuously with increasing pressure, as shown in Figure S8 of the Supporting Information. The diffraction pattern at 33.3 GPa could be fitted well to tetragonal $CsPb_2I_5$ (Figure 2c). The lattice parameters and cell volume of $CsPb_2I_5$ under high pressure are displayed in panels b and c of Figure 3. Different from $CsPb_2Br_5$ reported previously,[47] in which there is a sudden change at 1.6 GPa, all of the lattice constants show a continuous decrease during the compression in our case. The *c* axis is more compressible than *a* and *b* axes. The experimental pressure−volume data are fitted by the Birch−Murnaghan equation[48]

$$P(V) = \frac{3B_0}{2}\left[\left(\frac{V_0}{V}\right)^{7/3} - \left(\frac{V_0}{V}\right)^{5/3}\right]\left\{1 + \frac{3}{4}(B_0' - 4)\left[\left(\frac{V_0}{V}\right)^{2/3} - 1\right]\right\}$$

where V_0 is the unit cell volume at ambient pressure, V is the volume at pressure P, B_0 is the bulk modulus at ambient pressure, and B_0' is a parameter for the pressure derivative. The bulk modulus B_0 of $CsPb_2I_5$ is calculated to be about 29(1) GPa with B_0' fixed at 4 and V_0 = 1255(10) Å^3. The bulk modulus B_0 of $CsPb_2I_5$ is slightly larger than the *Pnma* and *C*2/*m* phases of $CsPbI_3$, in which B_0 is previously reported to be 27.7(2) and 18.6(3) GPa, respectively.[43] The result indicates that the compact layered structure of $CsPb_2I_5$ renders a less compressible lattice. The cell volume and lattice parameters of CsI are different from those of the previous study, which may be due to the space confinement effect of 2D $CsPb_2I_5$ as well as the nanosize effect of CsI itself.

Figure 4 shows the absorption spectra of $CsPb_2I_5$ at high pressures and the corresponding optical bandgap as a function of the pressure. The bandgaps of $CsPb_2I_5$ at different pressures were determined by extrapolating the linear portion of α^2 versus the $h\nu$ curve in Tauc plots (inset of Figure 4b), where α is the absorption coefficient and $h\nu$ is the photon energy. The recovered sample exhibits a steep absorbance at 520 nm with a corresponding optical bandgap of 2.38 eV, consistent with the calculated bandgap (2.22 eV) of $CsPb_2I_5$ in the theoretical study.[49] It should be noted that the bandgap of CsI is ∼5 eV,[46] far beyond that of $CsPb_2I_5$. This means that the occurrence of CsI in the sample did not affect the absorption behavior of $CsPb_2I_5$ (Figures S9 and S10 of the Supporting Information). Generally, the absorption edges exhibit a gradually red shift with the optical bandgap of $CsPb_2I_5$, shifting from 2.38 eV at 0 GPa to 1.68 eV at 18.6 GPa. Upon decompression, the bandgap change is quite monotonic with pressure releasing (Figure 4b). The detailed absorption spectrum and bandgap evolution decompressed from 36.9 GPa can be seen in Figures S11−S13 of the Supporting Information. Similar changes can also be traced from optical micrographs of $CsPb_2I_5$ during compression−decompression cycling in Figure 4c. At ambient conditions, the sample was pale yellow. With pressure increasing, the colors of the sample gradually became red and then transformed into black at above 16 GPa. In addition,

https://doi.org/10.1021/acs.jpclett.2c00116
J. Phys. Chem. Lett. 2022, 13, 2555−2562

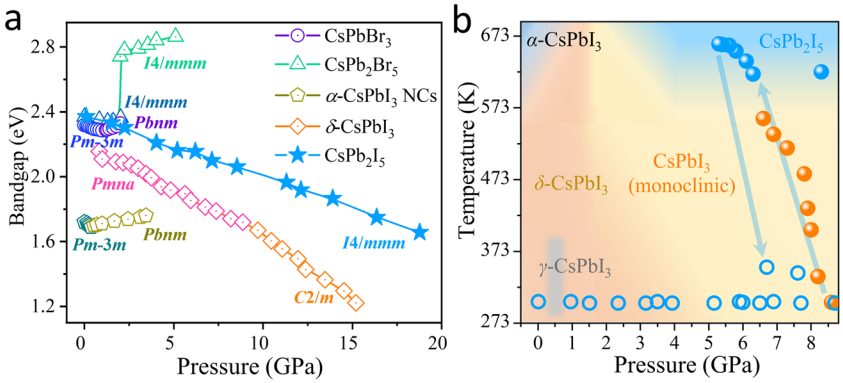

Figure 5. (a) Summary of the pressure-dependent bandgap of cesium lead halide perovskite and its derivatives. The color changes indicate structural phase transition. Data are from refs 43, 47, 50, and 51 and this work. (b) Experimental routes from the high-pressure phase of $CsPbI_3$ to $CsPb_2I_5$ at high $P-T$ conditions. The color shows different phases of $CsPbI_3$, i.e., the α phase (indigo), γ phase (gray, a thermodynamically metastable phase), δ phase (orange), high-pressure phase of δ-$CsPbI_3$ (yellow), and $CsPb_2I_5$ obtained in this work (blue).

$CsPb_2I_5$ with the tetrahedral structure shows no PL emission at either high pressure or ambient conditions.

The tunability of the bandgap in the metal halide perovskites with a stable structure is important for optoelectronic applications. As shown in Figure 5a, we summarize the pressure-dependent bandgap of cesium lead halide perovskite and its derivatives, including $CsPbBr_3$,[50] $CsPb_2Br_5$,[47] δ-$CsPbI_3$,[43] α-$CsPbI_3$ nanocrystals (NCs),[51] and newly reported $CsPb_2I_5$. Generally, most of these materials exhibit an abrupt change of the optical bandgap accompanied by the crystal structural transitions (Figure 5a). Interestingly, the layered phase of $CsPb_2I_5$ exhibits flexible bandgap tunability from 2.38 eV at ambient pressure to 1.68 eV at 18 GPa, while keeping the tetragonal structure stable upon compression. The superior bandgap tunability and highly stable structure endow $CsPb_2I_5$ with promising applications in optoelectronics and pressure sensors. Considering promising possibilities, $CsPb_2I_5$ could cooperate with $CsPbI_3$ to fabricate high-quality composites.

On the basis of the XRD and previous research of $CsPbI_3$, we tentatively show a $P-T$ phase diagram in Figure 5b for synthesis of $CsPb_2I_5$ by conversion of $CsPbI_3$. The formation of the α phase (high-temperature phase) and γ phase (thermodynamically metastable phase) can be transformed from the δ phase (low-temperature phase) of $CsPbI_3$ when the applied pressure is below 2 GPa, whereas the high $P-T$ conditions are required to synthesize $CsPb_2I_5$ by conversion of high-pressure monoclinic $CsPbI_3$. Once preserved to RT, tetragonal $CsPb_2I_5$ can be retained, even after fully releasing pressure to ambient conditions.

It should be noted that the halide perovskite ABX_3 can be a degradant at ambient conditions as a result of moisture and oxygen environmental sensitivity, following chemical equation: $ABX_3 \rightarrow AX + BX_2$. 2D AB_2X_5 has never been reported. Our work revealed for the first time that 2D $CsPb_2X_5$ can be obtained from $CsPbX_3$ under high $P-T$ conditions with the following pathway: $2CsPbX_3 \rightarrow CsPb_2X_5 + CsX$. In comparison to the traditional synthesis methods of $CsPb_2X_5$ with several raw materials, multiple chemical reaction steps, injected impurities, and defects, the synthesis of $CsPb_2I_5$ at high $P-T$ conditions is simple with a single chemical equation, and the product does not introduce new impurities.

Previous research reported that the perovskite ABX_3 (such as $NaMgF_3$[39]) will be dissociated into AB_2X_5 ($P2_1/c$ type) and AX (CsCl type) under high pressure. Theoretically, the calculation predicted the dissociations of ABX_3 to AB_2X_5 as an endothermic reaction, which is related to the increases of bond lengths of A−X and B−X across the dissociations with increases of cation coordination numbers. Longer bonds lead to smaller optic phonon frequencies and larger vibrational entropy, which results in the lower Gibbs free energy. Likewise, $CsPb_2I_5$ has longer Pb−I and Cs−I bonds than $CsPbI_3$ (please refer to the comparation of bond lengths between $CsPb_2I_5$ and $CsPbI_3$ in Table S1 of the Supporting Information). The structures of cesium lead halide perovskites $CsPbX_3$ are similar to $NaMgF_3$ under ambient conditions. Thus, the formation mechanism of $CsPb_2X_5$ may be similar to that of $NaMgF_3$, in which $CsPb_2I_5$ displays thermally structural stability with the lower Gibbs free energy than $CsPbI_3$. The present work also reveals that the synthesis of 2D $CsPb_2X_5$ by conversion of perovskite $CsPbX_3$ at high $P-T$ conditions is a universal phenomenon with common characteristics that can be expanded to all perovskite/perovskite-related ABX_3 systems. It also indicates that pure $CsPb_2I_5$ could be obtained by following the chemical reaction of $CsPbI_3 + PbI_2$ at high $P-T$ conditions.

In summary, we demonstrate the synthesis of 2D $CsPb_2X_5$ (X = Br and I) by the direct conversion of $CsPbX_3$ at high $P-T$ conditions. Obtained tetragonal $CsPb_2I_5$ is quenchable at ambient conditions, having the lattice constants of $a = b = 9.060(1)$ Å, $c = 15.901(2)$ Å, and $V = 1305.3(4)$ Å^3. The structural and optical properties under high pressures were systematically investigated using XRD and absorption spectroscopy. $CsPb_2I_5$ exhibits flexible optical properties while keeping the tetragonal structure stable up to 33.3 GPa. Further experiments demonstrate that typical 3D $CsPbBr_3$ with corner-shared $[PbBr_6]^{4-}$ octahedrons displays a similar structural transformation into 2D $CsPb_2Br_5$, indicating that the synthesis of 2D $CsPb_2X_5$ by conversion of $CsPbX_3$ at high $P-T$ conditions is a universal phenomenon with common characteristics that can be expanded to more perovskite systems. This work not only presents a new strategy for the synthesis of the perovskite derivatives at high $P-T$ conditions but also sheds light on the exploration of novel low-dimensional perovskite materials.

https://doi.org/10.1021/acs.jpclett.2c00116
J. Phys. Chem. Lett. 2022, 13, 2555−2562

■ ASSOCIATED CONTENT

Supporting Information

The Supporting Information is available free of charge at https://pubs.acs.org/doi/10.1021/acs.jpclett.2c00116.

Experimental details, including photographs of crystal structure details, HRTEM, SEM, refinement result of $CsPb_2Br_5$, *d* spacing and lattice parameter of $CsPb_2I_5$ and CsI, and optical properties of $CsPb_2I_5$ under high pressure (PDF)

Transparent Peer Review report available (PDF)

■ AUTHOR INFORMATION

Corresponding Authors

Chuanlong Lin − *Center for High Pressure Science and Technology Advanced Research (HPSTAR), Beijing 100094, People's Republic of China*; Email: chuanlong.lin@hpstar.ac.cn

Xujie Lü − *Center for High Pressure Science and Technology Advanced Research (HPSTAR), Beijing 100094, People's Republic of China*; orcid.org/0000-0001-8402-7160; Email: xujie.lu@hpstar.ac.cn

Authors

Mei Li − *Center for High Pressure Science and Technology Advanced Research (HPSTAR), Beijing 100094, People's Republic of China*

Shang Peng − *Center for High Pressure Science and Technology Advanced Research (HPSTAR), Beijing 100094, People's Republic of China*; orcid.org/0000-0001-5893-4082

Shiyu Fang − *School of Materials and Engineering, Shanghai Institute of Technology, Shanghai 200235, People's Republic of China*

Yu Gong − *Beijing Synchrotron Radiation Facility, Institute of High Energy Physics, Chinese Academy of Science, Beijing 100049, People's Republic of China*

Dongliang Yang − *Beijing Synchrotron Radiation Facility, Institute of High Energy Physics, Chinese Academy of Science, Beijing 100049, People's Republic of China*

Kejun Bu − *Center for High Pressure Science and Technology Advanced Research (HPSTAR), Beijing 100094, People's Republic of China*

Bingyan Liu − *Center for High Pressure Science and Technology Advanced Research (HPSTAR), Beijing 100094, People's Republic of China*

Hui Luo − *Center for High Pressure Science and Technology Advanced Research (HPSTAR), Beijing 100094, People's Republic of China*

Songhao Guo − *Center for High Pressure Science and Technology Advanced Research (HPSTAR), Beijing 100094, People's Republic of China*; orcid.org/0000-0003-0570-0164

Junlong Li − *Center for High Pressure Science and Technology Advanced Research (HPSTAR), Beijing 100094, People's Republic of China; Beijing Synchrotron Radiation Facility, Institute of High Energy Physics, Chinese Academy of Science, Beijing 100049, People's Republic of China*

Hao Wang − *Center for High Pressure Science and Technology Advanced Research (HPSTAR), Beijing 100094, People's Republic of China*

Yufeng Liu − *School of Materials and Engineering, Shanghai Institute of Technology, Shanghai 200235, People's Republic of China*; orcid.org/0000-0002-2733-7733

Sheng Jiang − *Shanghai Synchrotron Radiation Facility, Shanghai Advanced Research Institute, Chinese Academy of Science, Shanghai 201204, People's Republic of China*

Complete contact information is available at: https://pubs.acs.org/10.1021/acs.jpclett.2c00116

Notes

The authors declare no competing financial interest.

■ ACKNOWLEDGMENTS

The authors thank the financial support from the National Key Research and Development Program of China (Grant 2021YFB3702102), the National Natural Science Foundation of China (NSFC, Grants 11974033 and U2141240), and the Shanghai Natural Science Foundation (Grant 20ZR1455400). The XRD measurements were performed at the 4W2 HP-Station, Beijing Synchrotron Radiation Facility (BSRF), and beamline 15U1, Shanghai Synchrotron Radiation Facility (SSRF), which were supported by the Chinese Academy of Sciences (Grants KJCX2-SW-N03 and KJCX2-SW-N20).

■ REFERENCES

(1) Zhao, Y.; Zhu, K. Organic-Inorganic Hybrid Lead Halide Perovskites for Optoelectronic and Electronic Applications. *Chem. Soc. Rev.* **2016**, *45* (3), 655−689.

(2) Zhou, Y.; Chen, J.; Bakr, O. M.; Mohammed, O. F. Metal Halide Perovskites for X-ray Imaging Scintillators and Detectors. *ACS Energy Lett.* **2021**, *6* (2), 739−768.

(3) Friend, R. H.; Di, D.; Lilliu, S.; Zhao, B. Perovskite LEDs. *Sci. Video Protoc.* **2018**, *1* (1), 1−5.

(4) Wang, R.; Mujahid, M.; Duan, Y.; Wang, Z.-K.; Xue, J.; Yang, Y. A Review of Perovskites Solar Cell Stability. *Adv. Funct. Mater.* **2019**, *29* (47), 1808843.

(5) Kim, B.; Seok, S. Il. Molecular Aspects of Organic Cations Affecting the Humidity Stability of Perovskites. *Energy Environ. Sci.* **2020**, *13* (3), 805−820.

(6) Sun, Q.; Yin, W. J. Thermodynamic Stability Trend of Cubic Perovskites. *J. Am. Chem. Soc.* **2017**, *139* (42), 14905−14908.

(7) Tang, X.; Han, S.; Zu, Z.; Hu, W.; Zhou, D.; Du, J.; Hu, Z.; Li, S.; Zang, Z. All-Inorganic Perovskite $CsPb_2Br_5$ Microsheets for Photodetector Application. *Front. Phys.* **2018**, *5*, 69.

(8) Huang, Z. P.; Ma, B.; Wang, H.; Li, N.; Liu, R. T.; Zhang, Z. Q.; Zhang, X. D.; Zhao, J. H.; Zheng, P. Z.; Wang, Q.; Zhang, H. L. In Situ Growth of 3D/2D ($CsPbBr_3$/$CsPb_2Br_5$) Perovskite Heterojunctions toward Optoelectronic Devices. *J. Phys. Chem. Lett.* **2020**, *11* (15), 6007−6015.

(9) Wang, K.-H.; Wu, L.; Li, L.; Yao, H.-B.; Qian, H.-S.; Yu, S.-H. Large-Scale Synthesis of Highly Luminescent Perovskite-Related $CsPb_2Br_5$ Nanoplatelets and Their Fast Anion Exchange. *Angew. Chem., Int. Ed.* **2016**, *128* (29), 8468−8472.

(10) Lin, C.; Liu, L.; Xu, J.; Fang, F.; Jiang, K.; Liu, Z.; Wang, Y.; Chen, F.; Yao, H. Facile Synthesis of a Dual-Phase $CsPbBr_3$-$CsPb_2Br_5$ single Crystal and Its Photoelectric Performance. *RSC Adv.* **2020**, *10* (35), 20745−20752.

(11) Ruan, L.; Shen, W.; Wang, A.; Xiang, A.; Deng, Z. Alkyl-Thiol Ligand-Induced Shape- and Crystalline Phase-Controlled Synthesis of Stable Perovskite-Related $CsPb_2Br_5$ Nanocrystals at Room Temperature. *J. Phys. Chem. Lett.* **2017**, *8* (16), 3853−3860.

(12) Wang, C.; Wang, Y.; Su, X.; Hadjiev, V. G.; Dai, S.; Qin, Z.; Calderon Benavides, H. A.; Ni, Y.; Li, Q.; Jian, J.; Alam, M. K.; Wang, H.; Robles Hernandez, F. C.; Yao, Y.; Chen, S.; Yu, Q.; Feng, G.; Wang, Z.; Bao, J. Extrinsic Green Photoluminescence from the Edges of 2D Cesium Lead Halides. *Adv. Mater.* **2019**, *31* (33), 1902492.

(13) Li, J.; Zhang, H.; Wang, S.; Long, D.; Li, M.; Guo, Y.; Zhong, Z.; Wu, K.; Wang, D.; Zhang, T. Synthesis of All-Inorganic $CsPb_2Br_5$ Perovskite and Determination of Its Luminescence Mechanism. *RSC Adv.* **2017**, *7* (85), 54002−54007.
(14) Zhang, T.; Chen, Z.; Shi, Y.; Xu, Q.-H. The Photoluminescence Mechanism of $CsPb_2Br_5$ Microplates Revealed by Spatially Resolved Single Particle Spectroscopy. *Nanoscale* **2019**, *11* (7), 3186−3192.
(15) Turedi, B.; Lee, K. J.; Dursun, I.; Alamer, B.; Wu, Z.; Alarousu, E.; Mohammed, O. F.; Cho, N.; Bakr, O. M. Water-Induced Dimensionality Reduction in Metal-Halide Perovskites. *J. Phys. Chem. C* **2018**, *122* (25), 14128−14134.
(16) Iyikanat, F.; Sari, E.; Sahin, H. Thinning $CsPb_2Br_5$ Perovskite down to Monolayers: Cs-Dependent Stability. *Phys. Rev. B* **2017**, *96* (15), 155442.
(17) Cao, M.; Damji, Y.; Zhang, C.; Wu, L.; Zhong, Q.; Li, P.; Yang, D.; Xu, Y.; Zhang, Q. Low-Dimensional-Networked Cesium Lead Halide Perovskites: Properties, Fabrication, and Applications. *Small Methods* **2020**, *4* (12), 2000303.
(18) Li, G.; Wang, H.; Zhu, Z.; Chang, Y.; Zhang, T.; Song, Z.; Jiang, Y. Shape and Phase Evolution from $CsPbBr_3$ Perovskite Nanocubes to Tetragonal $CsPb_2Br_5$ Nanosheets with an Indirect Bandgap. *Chem. Commun.* **2016**, *52* (75), 11296−11299.
(19) Dutta, A.; Behera, R. K.; Dutta, S. K.; Das Adhikari, S.; Pradhan, N. Annealing $CsPbX_3$ (X = Cl and Br) Perovskite Nanocrystals at High Reaction Temperatures: Phase Change and Its Prevention. *J. Phys. Chem. Lett.* **2018**, *9* (22), 6599−6604.
(20) Acharyya, P.; Pal, P.; Samanta, P. K.; Sarkar, A.; Pati, S. K.; Biswas, K. Single Pot Synthesis of Indirect Band Gap 2D $CsPb_2Br_5$ Nanosheets from Direct Band Gap 3D $CsPbBr_3$ Nanocrystals and the Origin of Their Luminescence Properties. *Nanoscale* **2019**, *11* (9), 4001−4007.
(21) Pradhan, N. Tips and Twists in Making High Photoluminescence Quantum Yield Perovskite Nanocrystals. *ACS Energy Lett.* **2019**, *4* (7), 1634−1638.
(22) Tan, Y.; Li, R.; Xu, H.; Qin, Y.; Song, T.; Sun, B. Ultrastable and Reversible Fluorescent Perovskite Films Used for Flexible Instantaneous Display. *Adv. Funct. Mater.* **2019**, *29* (23), 1900730.
(23) Liu, M.; Zhao, J.; Luo, Z.; Sun, Z.; Pan, N.; Ding, H.; Wang, X. Unveiling Solvent-Related Effect on Phase Transformations in CsBr-$PbBr_2$ System: Coordination and Ratio of Precursors. *Chem. Mater.* **2018**, *30* (17), 5846−5852.
(24) Kostopoulou, A.; Vernardou, D.; Savva, K.; Stratakis, E. All-Inorganic Lead Halide Perovskite Nanohexagons for High Performance Air-Stable Lithium Batteries. *Nanoscale* **2019**, *11* (3), 882−889.
(25) Sandeep, K.; Gopika, K. Y.; Revathi, M. R. Role of Capped Oleyl Amine in the Moisture-Induced Structural Transformation of $CsPbBr_3$ Perovskite Nanocrystals. *Phys. Status Solidi RRL* **2019**, *13* (11), 1900387.
(26) Maity, G.; Pradhan, S. K. Composition Related Structural Transition between Mechanosynthesized $CsPbBr_3$ and $CsPb_2Br_5$ Perovskites and Their Optical Properties. *J. Alloys Compd.* **2020**, *816*, 152612.
(27) Balakrishnan, S. K.; Kamat, P. V. Ligand Assisted Transformation of Cubic $CsPbBr_3$ Nanocrystals into Two-Dimensional $CsPb_2Br_5$ Nanosheets. *Chem. Mater.* **2018**, *30* (1), 74−78.
(28) Kususe, Y.; Yoshida, S.; Fujita, K.; Akamatsu, H.; Fukuzumi, M.; Murai, S.; Tanaka, K. Structural Phase Transitions in $EuNbO_3$ Perovskite. *J. Solid State Chem.* **2016**, *239*, 192−199.
(29) Lin, C.; Liu, J.; Lin, J.; Li, X.; Li, Y.; Zhang, Q.; Xiong, L.; Li, R. Garnet-to-Perovskite Transition in $Gd_3Sc_2Ga_3O_{12}$ at High Pressure and High Temperature. *Inorg. Chem.* **2013**, *52* (1), 431−434.
(30) Lin, C.; Liu, J.; Li, X.; Li, Y.; Chu, S.; Xiong, L.; Li, R. Phase Transformation in Hexagonal $ErMnO_3$ under High Pressure. *J. Appl. Phys.* **2012**, *112* (11), 113512.
(31) Guo, S.; Zhao, Y.; Bu, K.; Fu, Y.; Luo, H.; Chen, M.; Hautzinger, M. P.; Wang, Y.; Jin, S.; Yang, W.; Lü, X. Pressure-Suppressed Carrier Trapping Leads to Enhanced Emission in Two-Dimensional Perovskite $(HA)_2(GA)Pb_2I_7$. *Angew. Chem., Int. Ed.* **2020**, *132* (40), 17686−17692.
(32) Luo, H.; Guo, S.; Zhang, Y.; Bu, K.; Lin, H.; Wang, Y.; Yin, Y.; Zhang, D.; Jin, S.; Zhang, W.; Yang, W.; Ma, B.; Lü, X. Regulating Exciton−Phonon Coupling to Achieve a Near-Unity Photoluminescence Quantum Yield in One-Dimensional Hybrid Metal Halides. *Adv. Sci.* **2021**, *8* (14), 2100786.
(33) Wang, Y.; Guo, S.; Luo, H.; Zhou, C.; Lin, H.; Ma, X.; Hu, Q.; Du, M. H.; Ma, B.; Yang, W.; Lü, X. Reaching 90% Photoluminescence Quantum Yield in One-Dimensional Metal Halide $C_4N_2H_{14}PbBr_4$ by Pressure-Suppressed Nonradiative Loss. *J. Am. Chem. Soc.* **2020**, *142* (37), 16001−16006.
(34) Li, Q.; Zhang, L.; Chen, Z.; Quan, Z. Metal Halide Perovskites under Compression. *J. Mater. Chem. A* **2019**, *7* (27), 16089−16108.
(35) Li, M.; Liu, T.; Wang, Y.; Yang, W.; Lü, X. Pressure Responses of Halide Perovskites with Various Compositions, Dimensionalities, and Morphologies. *Matter Radiat. at Extrems* **2020**, *5* (1), 018201.
(36) Liu, G.; Kong, L.; Yang, W.; Mao, H.-k. Pressure Engineering of Photovoltaic Perovskites. *Mater. Today* **2019**, *27*, 91−106.
(37) Guo, S.; Bu, K.; Li, J.; Hu, Q.; Luo, H.; He, Y.; Wu, Y.; Zhang, D.; Zhao, Y.; Yang, W.; Kanatzidis, M. G.; Lü, X. Enhanced Photocurrent of All-Inorganic Two-Dimensional Perovskite $Cs_2PbI_2Cl_2$ via Pressure-Regulated Excitonic Features. *J. Am. Chem. Soc.* **2021**, *143* (6), 2545−2551.
(38) Umemoto, K.; Wentzcovitch, R. M. Two-Stage Dissociation in $MgSiO_3$ Post-Perovskite. *Earth Planet. Sci. Lett.* **2011**, *311* (3−4), 225−229.
(39) Dutta, R.; Greenberg, E.; Prakapenka, V. B.; Duffy, T. S. Phase Transitions beyond Post-Perovskite in $NaMgF_3$ to 160 GPa. *Proc. Natl. Acad. Sci. U. S. A.* **2019**, *116* (39), 19324−19329.
(40) Umemoto, K.; Wentzcovitch, R. M. *Ab Initio* Exploration of Post-PPV Transitions in Low-Pressure Analogs of $MgSiO_3$. *Phys. Rev. Mater.* **2019**, *3* (12), 123601.
(41) Stoumpos, C. C.; Malliakas, C. D.; Kanatzidis, M. G. Semiconducting Tin and Lead Iodide Perovskites with Organic Cations: Phase Transitions, High Mobilities, and near-Infrared Photoluminescent Properties. *Inorg. Chem.* **2013**, *52* (15), 9019−9038.
(42) Ke, F.; Wang, C.; Jia, C.; Wolf, N. R.; Yan, J.; Niu, S.; Devereaux, T. P.; Karunadasa, H. I.; Mao, W. L.; Lin, Y. Preserving a Robust $CsPbI_3$ Perovskite Phase via Pressure-Directed Octahedral Tilt. *Nat. Commun.* **2021**, *12* (1), 461.
(43) Liang, Y.; Huang, X.; Huang, Y.; Wang, X.; Li, F.; Wang, Y.; Tian, F.; Liu, B.; Shen, Z. X.; Cui, T. New Metallic Ordered Phase of Perovskite $CsPbI_3$ under Pressure. *Adv. Sci.* **2019**, *6* (14), 1900399.
(44) Yuan, G.; Qin, S.; Wu, X.; Ding, H.; Lu, A. Pressure-Induced Phase Transformation of $CsPbI_3$ by X-ray Diffraction and Raman Spectroscopy. *Phase Transit* **2018**, *91* (1), 38−47.
(45) Lü, X.; Stoumpos, C.; Hu, Q.; Ma, X.; Zhang, D.; Guo, S.; Hoffman, J.; Bu, K.; Guo, X.; Wang, Y.; Ji, C.; Chen, H.; Xu, H.; Jia, Q.; Yang, W.; Kanatzidis, M. G.; Mao, H.-K. Regulating Off-Centering Distortion Maximizes Photoluminescence in Halide Perovskites. *Natl. Sci. Rev.* **2021**, *8* (9), nwaa288.
(46) Asaumi, K. Pressure-Induced Successive Phase Transitions in CsI and Its Equation of State in Relation to Metallization. *Phys. Rev. B* **1984**, *29* (2), 1118−1120.
(47) Ma, Z.; Li, F.; Qi, G.; Wang, L.; Liu, C.; Wang, K.; Xiao, G.; Zou, B. Structural Stability and Optical Properties of Two-Dimensional Perovskite-like $CsPb_2Br_5$ Microplates in Response to Pressure. *Nanoscale* **2019**, *11* (3), 820−825.
(48) Birch, F. Finite Elastic Strain of Cubic Crystals. *Phys. Rev.* **1947**, *71* (11), 809−824.
(49) Zhang, B.; Zhang, H.; Lin, J.; Cheng, X. A Time-Dependent Density Functional Study on Optical Response in All-Inorganic Lead-Halide Perovskite Nanostructures. *Int. J. Quantum Chem.* **2020**, *120* (13), e26232.
(50) Zhang, L.; Zeng, Q.; Wang, K. Pressure-Induced Structural and Optical Properties of Inorganic Halide Perovskite $CsPbBr_3$. *J. Phys. Chem. Lett.* **2017**, *8* (16), 3752−3758.
(51) Cao, Y.; Qi, G.; Liu, C.; Wang, L.; Ma, Z.; Wang, K.; Du, F.; Xiao, G.; Zou, B. Pressure-Tailored Band Gap Engineering and

Structure Evolution of Cubic Cesium Lead Iodide Perovskite Nanocrystals. *J. Phys. Chem. C* **2018**, *122* (17), 9332−9338.

https://doi.org/10.1021/acs.jpclett.2c00116
J. Phys. Chem. Lett. 2022, 13, 2555−2562